Spatially Resolved Transient Dynamics of Charge Density Waves in $NbSe_3$

E. C. Geil and R. E. Thorne
Laboratory of Atomic and Solid State Physics, Cornell University, Ithaca, New York 14853, USA
(Received 25 June 2014; published 7 January 2015)

We have developed methods for acquiring temporally and spatially resolved spectrograms of the velocity of sliding charge-density waves (CDWs), allowing unprecedented access to CDW dynamics. Complex transients arising from the interplay between elastic and plastic processes occur when the driving field direction is reversed. A transient spectral component due to shear elasticity can be unambiguously identified, and allows the most direct determination to date of the CDW's shear elastic modulus. Near current contacts, initially elastic displacements are followed by an elastic-to-plastic transition. A simple model provides a semiquantitative account of many aspects of these transients.

DOI: 10.1103/PhysRevLett.114.016404 PACS numbers: 71.45.Lr

In quasi-one-dimensional conductors such as $NbSe_3$ collective charge transport by incommensurate charge- or spin-density waves manifests in a diverse array of electronic properties [1]. Coupling of a charge-density wave's (CDW's) phase $\phi(r,t)$ to impurities leads to a threshold electric field E_T for the onset of CDW "sliding." For a perfectly elastic CDW, the sliding state at a given $E > E_T$ is predicted to be asymptotically unique and $\phi(\mathbf{r},t)$ to exhibit locally and globally periodic evolution in time [2]. This leads to voltage oscillations at a "washboard" frequency $f_c = d\phi/dt = v_c/\lambda_c \propto j_c$, where v_c, λ_c, and j_c are the CDW velocity, wavelength, and current density, respectively, with f_c ranging from kHz just above E_T to GHz at $E \sim 200E_T$ [3,4].

However, plasticity plays two crucial roles in the dynamics of real CDW conductors. First, conversion between single-particle and collective currents must occur near current contacts. For $E > E_T$, longitudinal strains [5–8] drive phase slip [9–12]—the addition and removal of CDW wave fronts. Phase slip can extend from ~ 10 μm to ~ 1 mm inward from current contacts, leading to longitudinal variations in v_c on this scale [13,14].

Second, sample inhomogeneities can result in shear deformations and in shear slip. For sample thicknesses less than ~ 10 μm, E_T and the strength of collective pinning increases with decreasing thickness [15]. Thickness variations transverse to the CDW sliding direction (e.g., arising from small-angle grain boundaries) thus cause shear stress [16–18], and shear slip can cause transverse variations in v_c and j_c [19].

Together, these processes destroy the steady sliding state's homogeneity and periodicity, and lead to spatiotemporally complex transient dynamics. Transient CDW dynamics has primarily been probed using i-v measurements [1,13,20,21]. The CDW current between voltage contacts is estimated as $i_c(t) = i(t) - v(t)/R_n$, where R_n is the single particle resistance measured below E_T. This estimate spatially averages over the sample width and voltage contact separation. It also assumes that R_n is constant, independent of current i and time t, valid just below the Peierls transition temperature T_P but inadequate below $T \approx T_P/2$, especially for materials like TaS_3 and $K_{0.3}MoO_3$ whose Fermi surfaces are fully gapped by CDW formation.

In principle, the most direct way to probe CDW dynamics is via measurements of voltage oscillations near the washboard frequency f_c, as these reveal the distribution and fluctuations of the local CDW velocity. Using high-performance cryogenic amplifiers and arrays of voltage contacts, we have followed the position-dependent time evolution of the CDW velocity spectrum in response to pulsed applied currents. This approach allows unprecedented access to transient CDW dynamics.

High purity $NbSe_3$ crystals were laid atop gold contact arrays micropatterned on alumina substrates as shown Fig. 1. The two current contacts were each at least 100 μm wide. The 2 μm wide voltage contacts were

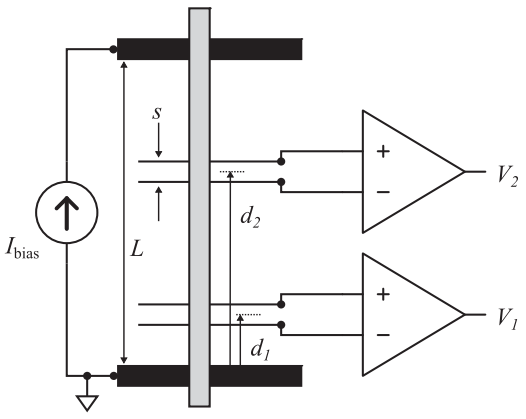

FIG. 1. Experimental configuration. Current pulses are applied to a $NbSe_3$ crystal, and voltages across any two voltage contact pairs are simultaneously measured using two cryogenic differential amplifiers. For all crystals, the crystallographic b and c axes were along the length L and width, respectively.

nonperturbing [14]. Contacts within a pair were separated by $s = 50$ μm. Voltages across any two contact pairs could be simultaneously measured using two amplifiers.

Previous CDW transient response studies [1,13,20] used room-temperature amplifiers. Large contact resistances ($\sim$1 kΩ) and wiring capacitances ($\sim$100 pF) limit bandwidths to $\sim$1 MHz; high impedance sample signals are susceptible to interference; and thermal amplifier noise is significant. To address these problems, we designed and implemented amplifiers having a symmetrical, fully differential cryogenic input stage. The amplifiers have an overall gain of 300 V/V, a 3 dB bandwidth of 60 MHz, a CMRR of 90 dB at 1 MHz, and a noise floor of 0.9 nV Hz$^{-1/2}$ at 77 K (the cryogenic stage's temperature during measurements).

To resolve transients in both frequency and time, we compute the spectrogram of each voltage signal,

$$S(t,f) = \left| \int_{-\infty}^{\infty} w(\tau - t) V(\tau) e^{-2\pi i f \tau} d\tau \right|^2, \qquad (1)$$

where $w(t)$ is a window function. To reduce noise, spectrograms were averaged over many repetitions of the driving pulse sequence; single-shot spectrograms indicated little or no shot-to-shot variation in the signals of interest. Additional sample and measurement details are given in the Supplemental Material [22].

The spectrogram in Fig. 2 shows the response of sample 1 ($L = 3$ mm) at $T = 90$ K to a periodic current pulse train, measured with a voltage contact pair at $d_1 = 1100$ μm, far from either current contact. The pulse magnitudes are $3.2I_T$, and the pulse polarity is reversed after every second pulse. The spectrogram exhibits several notable features. First is the pulse-sign-memory effect—a transient overshoot of the CDW velocity [20] (directly measured here via the washboard frequency f_c) when the preceding pulse has an opposite sign. The characteristic time for this transient ($\sim$100 μs) is much larger than the sample and wiring's RC time constant ($\sim$10 ns).

Second, the dynamics are asymmetric with respect to the CDW sliding direction. A larger transient overshoot is observed at $d_1 = 1100$ μm when the (negatively charged) CDW is driven toward the closest current contact (by $I < -I_T$) after being driven toward the farthest current contact (by $I > +I_T$), than for the opposite drive sequence. This reflects an intrinsic asymmetry in CDW phase slip [12,14,22].

Third, immediately after each current reversal, the washboard frequency spectrum initially broadens and splits into multiple subpeaks (most clearly visible when I switches from negative to positive). Over a time of $\sim$500 μs, this broadening collapses into a single sharp peak. Successive pulses of the same sign do not produce this transient broadening.

CDW dynamics close to current contacts is modified by phase slip required for current conversion. Figure 3 shows the response of sample 2 ($L = 1$ mm) at $T = 85$ K to

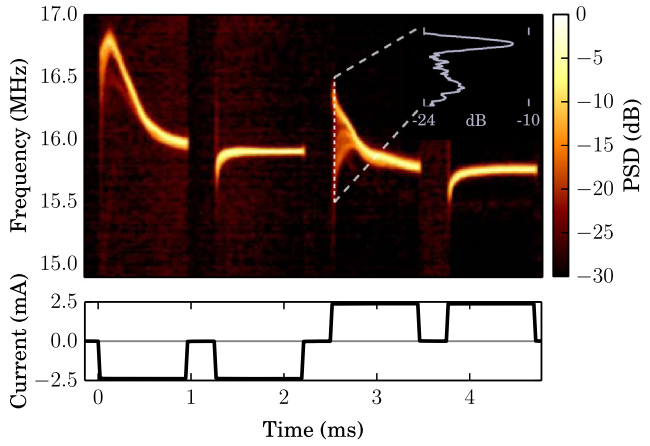

FIG. 2 (color online). Spectrogram of voltage across a contact pair near the middle of sample 1, measured in response to the periodic bias current shown in the lower panel. Note the transient spectral broadening at the start of each pulse and the asymmetry with respect to bias current direction. The inset shows the power spectral density (PSD) of the washboard frequency peak 50 μs after the beginning of the third pulse. The steady-state FWHM was approximately 20 kHz, corresponding to a quality factor of 800.

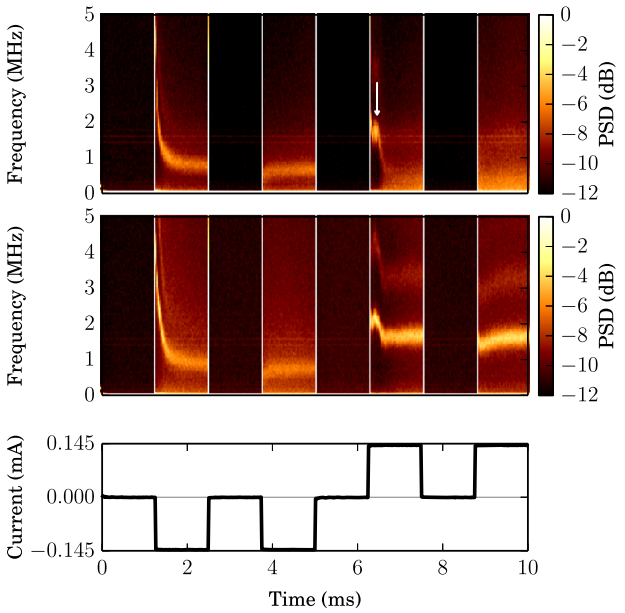

FIG. 3 (color online). Spectrogram of power spectral density (PSD) of voltage across contacts at (top, pair 1) $d_1 = 75$ μm and (middle, pair 2) $d_2 = 175$ μm from the lower current contact in Fig. 1, in response to the bias current pulses shown in the bottom panel. For the first positive current pulse, the spectral peak for pair 2 is initially sharp, but 250 μs later it undergoes a sudden broadening and a steep drop in mean frequency. The steady-state spectral FWHM was approximately 250 and 300 kHz for positive and negative current pulses, respectively.

current pulses of magnitude $1.45I_T$, measured between voltage contact pairs centered at $d_1 = 75$ μm (pair 1) and $d_2 = 175$ μm (pair 2) from the lower current contact in Fig. 1. This sample exhibits transient overshoots at both contacts pairs, but not the initial peak splitting seen in sample 1. The CDW segment between pair 1, closest to the current contact (and, less prominently, between pair 2) shows an additional feature not seen in sample 1's response far from the current contact: the velocity at the start of the transient is highly coherent, but 250 μs after the start of the positive pulse (indicated by the arrow), the mean washboard frequency drops to 300 kHz and the spectral width broadens dramatically. This suggests that the initial dynamics are elastic, but at 250 μs an elastic limit is exceeded, and phase slip begins. As in Fig. 2 for sample 1, the transients are strongly asymmetric with respect to current direction, and the loss of coherence on direction reversal is most pronounced when the CDW is sliding *towards* the nearby current contact.

What are the origins of the transient broadening of the CDW washboard frequency distribution in Fig. 2, and of the transition from elastic to steady-state plastic behavior in Fig. 3? CDW spectrogram peak broadening may arise in at least two ways: from longitudinal velocity gradients ($\partial v/\partial z \neq 0$) caused by phase slip and current conversion near current contacts; and from transverse velocity gradients ($\partial v/\partial x \neq 0$ or $\partial v/\partial y \neq 0$) associated with CDW shear dynamics (where x, y, and z are along the sample width, thickness, and length, respectively.)

For the transient data in Fig. 2, acquired far from the current contacts, longitudinal velocity gradients should be negligible. In the third pulse of Fig. 2, the most distant subpeaks are initially separated by $\Delta f \approx 300$ kHz, and they merge after a time $\Delta t \approx 250$ μs. If longitudinal v_c gradients caused this peak splitting, the minimum strain developed within the contact pair separation s in a time Δt would be $\epsilon_z \approx \frac{1}{2}(\Delta f)(\Delta t)\lambda/s \approx 1 \times 10^{-3}$. This is larger than even the largest longitudinal strains observed in $NbSe_3$ which occur *immediately adjacent* to current contacts [5,7,8]; the longitudinal strain decreases rapidly away from the contacts [12,13].

Consequently, we ascribe the initial broadening and subsequent narrowing of the peaks in Fig. 2 to shear strain transients and associated velocity shear. If adjacent transverse CDW regions have different pinning strengths, when a current pulse is applied they will initially slide at different velocities. Shear strain then develops and, if the elastic shear limit is not reached, eventually leads to a common sliding velocity. When the applied current returns to zero, pinning prevents relaxation of this shear strain [25]. When a current pulse of opposite sign is then applied, the initial shear stress propels the more weakly pinned regions forward, leading to a large initial velocity distribution, which then collapses as shear strain of the opposite sign accumulates.

The spectrograms in Fig. 2 allow us to estimate both the magnitude of the steady-state shear strain and the CDW's shear elastic modulus. Since sample 1's width is ~170 times larger than its thickness, the dominant shear component must be in the width (x) direction. The maximum shear strain calculated using the initial frequency splitting $\Delta f \approx 300$ kHz and the peak merging time $\Delta t \approx 250$ μs is $\gamma_{xz} \sim \frac{1}{2}(\Delta f)(\Delta t)\lambda/w = 8 \times 10^{-4}$. This value is comparable to CDW shear strains in $NbSe_3$ measured by x-ray microbeam diffraction [17].

To estimate the CDW's shear modulus, we consider a simplified two-dimensional version of the Fukuyama-Lee-Rice model [26],

$$\gamma \frac{\partial \phi}{\partial t} = K_x \frac{\partial^2 \phi}{\partial x^2} + K_z \frac{\partial^2 \phi}{\partial z^2} + \left(\frac{en_c}{Q}\right)(E - E_p), \quad (2)$$

where $E_p(j_c)$ is a phenomenological pinning field determined from the sample's I-V characteristic [13]. We assume that E_P is independent of bias for $I \gg I_T$ [13], but allow E_P to vary in the width (x) direction (e.g., due to transverse sample thickness variations). We analyze the dynamics in a frame moving with the steady-state CDW velocity, where $\partial\phi/\partial t$ describes only the transient evolution of ϕ and where $\int_{-w/2}^{w/2}[E - E_p(x)]dx = 0$. Since $\partial^2\phi/\partial z^2 \approx 0$ far from current contacts [5,7,8,13], the phase evolution then satisfies a heat equation,

$$\frac{\partial \phi}{\partial t} = \frac{K_x}{\gamma}\frac{\partial^2 \phi}{\partial x^2} + \left(\frac{en_c}{Q\gamma}\right)[E - E_p(x)], \quad (3)$$

where the shear stress $\partial\phi/\partial z$ vanishes at the sample edges ($x = 0, w$) [15,17]. Equation (3) can be solved using an eigenfunction expansion,

$$\phi(x,t) = \sum_{n=1}^{\infty} T_n(t)\cos(n\pi x/w),$$
$$T_n(t) = a_n e^{-t/\tau_n} + \beta_n \tau_n (1 - e^{-t/\tau_n}), \quad (4)$$

where $a_n = (2/w)\int_0^w \phi(t=0)\cos(n\pi x/w)dx$, $\beta_n = 2en_c/(wQ\gamma)\int_0^w [E - E_p(x)]\cos(n\pi x/w)dx$, and $\tau_n = (w/\pi n)^2 \times (\gamma/K_x)$ are the time constants for the phase evolution.

The time scale τ_s for the elastic shear transient is determined primarily by the slowest time constant,

$$\tau_s \approx \tau_1 = \frac{w^2\gamma}{\pi^2 K_x}. \quad (5)$$

Consistent with Eq. (5), the measured τ_s for sample 1 showed no discernible variation with current pulse magnitude for washboard frequencies from 1 to 25 MHz. Since $\gamma = \rho_c(en_c/Q)^2$, where ρ_c is the limiting high-field CDW resistivity, the shear modulus can then be determined as $G_{xz} = Q^2 K_x = (en_c w)^2 \rho_c/\tau_s$. Substituting measured

values for sample 1 at 90 K ($\rho_c = 5.8 \times 10^{-6}$ Ω m, $w = 72$ μm, $\tau_s = 200$ μs), the CDW shear modulus is estimated as $G_{xz} \sim 1.4 \times 10^7$ N/m^2. This is comparable to values estimated by scaling the longitudinal elastic constant K_z [5,8] by the CDW correlation length anisotropy, and from the change in the total shear modulus of $NbSe_3$ upon CDW depinning [27]. The present data give the most direct determination to date of the CDW shear modulus in the sliding state.

The transverse variation in E_p across the sample width can be estimated from the frequency broadening at the start of the transient Δf. Using the approximation $E - E_p(x) = \Delta E_p \cos(\pi x/w)$, the present model gives $\Delta E_p = \frac{1}{2}(\Delta f)\pi e n_c \rho_c / Q$. Using the measured Δf for sample 1 gives $\Delta E_p \sim 0.12$ V/m, a factor of 160 less than the threshold field $E_T = 19$ V/m. This small transverse variation in pinning field is consistent with sample 1's optically smooth surfaces and with its narrow steady-state spectral width.

The present model also explains the concentration of spectral density near the frequency extremes of the transiently broadened peak in Fig. 2. For $E - E_p(x) = \Delta E_p \cos(\pi x/w)$, the washboard frequency has an arcsine distribution $[\pi\sqrt{\hat{f}(1-\hat{f})}]^{-1}$, where $\hat{f} = (f_c - f_{c,\min})/(\Delta f)$. This spectral concentration persists even when higher order terms in the Fourier expansion are included, because $\partial f/\partial x$ must vanish at the sample edges (and at any interior extrema).

In contrast with the transient peak broadening seen near the middle of sample 1 in Fig. 2, the steady-state peak broadening and apparent elastic-to-plastic transition seen near a current contact of sample 2 in Fig. 3 cannot be due to shear dynamics. Sample 2's width w is eight times smaller than that of sample 1, so by Eq. (5) the time constant τ_s of its shear transient should be 64 times smaller, ~3 μs, much smaller than the observed 250 μs elastic transient in Fig. 3. Second, when the current is reversed, built-up shear strains act to maximize the peak broadening at the start of the transient, but the transient in Fig. 3 is most coherent there. Finally, the steady-state broadening observed at contact pair 2, only 50 μm from pair 1, is much smaller, and no broadening is observed at pairs farther from the current contact.

Consequently, the elastic-to-plastic transition in Fig. 3 must be associated with longitudinal strains and phase slip. An applied pulse compresses the CDW near the positive contact and stretches it near the negative contact; phase slip occurs near contacts, where the stress is largest. When the applied current direction is reversed, built-up stress drives the CDW toward the opposite polarization, leading to an elastic transient overshoot of the CDW velocity beyond its steady state value. As the stress near the current contacts grows, eventually phase slip begins, the CDW velocity and f_c decay with position z as the contacts are approached, and the longitudinal velocity gradient causes broadening of the washboard frequency peak, as seen in Fig. 3.

The maximum longitudinal strain at pair 1 in Fig. 3 can be estimated from the initial peak frequency $f_0 \approx 1.6$ MHz, the time $\Delta t \approx 250$ μs before the onset of slip, and the distance $L = 1000$ μm between current contacts as $\epsilon \approx [2\pi f_0(\Delta t)]/Ql = 6 \times 10^{-4}$. This is in good agreement with the $\epsilon \approx 5 \times 10^{-4}$ found by x-ray diffraction measurements [7,12] under similar conditions.

The transient jump in mean frequency seen on drive reversal in both Figs. 2 and 3 is due to longitudinal, current-conversion-related strains, whereas the transient peak broadening seen in Fig. 2 is due to shear strains. To more fully account for the behavior in Fig. 2, we have extended the 1D model of Ref. [13] describing longitudinal strain and slip to include elastic shear. The phase dynamics are described by

$$\frac{\partial\theta}{\partial t} = \left(\frac{Q}{en_c}\right)\frac{1}{\rho_c + \rho_p}\left[\rho_s j_{\rm tot} - E_p(x) + \frac{Q}{en_c}\left(K_x\frac{\partial^2\theta}{\partial x^2} + K_z\frac{\partial^2\theta}{\partial z^2}\right)\right] - \int_{-\infty}^{z} r_{\rm ps}[\theta(x,z',t)]dz', \tag{6}$$

where $\theta(x,z,t)$ is a renumbered phase, A is the cross-sectional area, and $j_{\rm tot}$ is the total sample current density. The phase slip rate per unit length is assumed to have the form $|r_{\rm ps}| = r_0 \exp(-t_{\rm ps}/|\partial\theta/\partial z|)$, with $r_0 \approx 1.0 \times 10^{11}$ m^{-1} s^{-1} and $t_{\rm ps} \sim 1.0 \times 10^7$ m^{-1}, determined in Ref. [13] from experimental fits. Figure 4 shows the results obtained by integrating Eq. (6), assuming $\Delta E_p = 0.12$ V/m and other parameters as deduced above. The simulation quantitatively reproduces the observed initial peak splitting and subsequent convergence, along with the overall transient excess velocity.

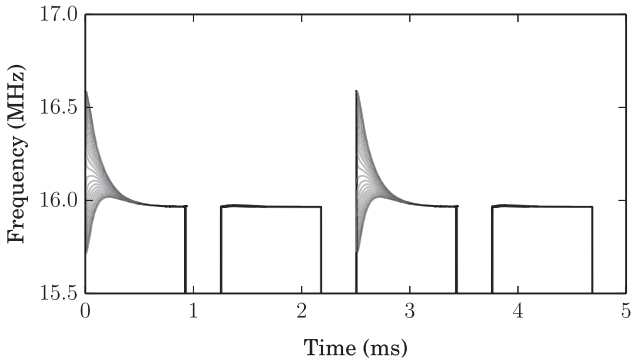

FIG. 4. Calculated local washboard frequencies at 30 uniformly spaced positions across the width of a sample, in response to the bias current profile of Fig. 2, calculated using Eq. (6) and parameters deduced from measurements on sample 1, as described in the text.

The present experiments indicate the exceptional promise of temporally and spatially resolved studies using high-performance cryogenic amplifiers for studying the elastic and plastic dynamics of driven density waves. These methods will be particularly enabling for the study of CDW velocity dynamics in fully gapped CDW materials at $T < T_P/2$, where coupling with single particle properties has largely obscured the collective contribution in conventional transport measurements.

This work was supported by the National Science Foundation under Grant No. DMR-0805240. Substrates were fabricated at the Cornell NanoScale Facility, a member of the National Nanotechnology Infrastructure Network, which is supported by the National Science Foundation (Grant No. ECCS-0335765).

[1] P. Monceau, Adv. Phys. **61**, 325 (2012).
[2] A. A. Middleton, Phys. Rev. Lett. **68**, 670 (1992).
[3] R. E. Thorne, W. G. Lyons, J. W. Lyding, J. R. Tucker, and J. Bardeen, Phys. Rev. B **35**, 6348 (1987).
[4] Y. I. Latyshev and V. E. Minakova, Synth. Met. **29**, 427 (1989).
[5] D. DiCarlo, E. Sweetland, M. Sutton, J. D. Brock, and R. E. Thorne, Phys. Rev. Lett. **70**, 845 (1993).
[6] M. E. Itkis, B. M. Emerling, and J. W. Brill, Phys. Rev. B **52**, R11545 (1995).
[7] H. Requardt, F. Y. Nad, P. Monceau, R. Currat, J. E. Lorenzo, S. Brazovskii, N. Kirova, G. Grübel, and C. Vettier, Phys. Rev. Lett. **80**, 5631 (1998).
[8] D. Rideau, P. Monceau, R. Currat, H. Requardt, F. Nad, J. E. Lorenzo, S. Brazovskii, C. Detlefs, and G. Grübel, Nucl. Instrum. Methods Phys. Res., Sect. A, **467–468**, 1010 (2001).
[9] N. P. Ong and K. Maki, Phys. Rev. B **32**, 6582 (1985).
[10] S. Ramakrishna, M. P. Maher, V. Ambegaokar, and U. Eckern, Phys. Rev. Lett. **68**, 2066 (1992).
[11] J. C. Gill, Phys. Rev. B **53**, 15586 (1996).
[12] S. Brazovskii, N. Kirova, H. Requardt, F. Y. Nad, P. Monceau, R. Currat, J. E. Lorenzo, G. Grubel, and C. Vettier, Phys. Rev. B **61**, 10640 (2000).
[13] T. L. Adelman, M. C. de Lind van Wijngaarden, S. V. Zaitsev-Zotov, D. DiCarlo, and R. E. Thorne, Phys. Rev. B **53**, 1833 (1996).
[14] S. G. Lemay, M. C. de Lind van Wijngaarden, T. L. Adelman, and R. E. Thorne, Phys. Rev. B **57**, 12781 (1998).
[15] J. McCarten, D. A. DiCarlo, M. P. Maher, T. L. Adelman, and R. E. Thorne, Phys. Rev. B **46**, 4456 (1992).
[16] Y. Li, S. G. Lemay, J. H. Price, K. Cicak, K. O'Neill, K. Ringland, K. D. Finkelstein, J. D. Brock, and R. E. Thorne, Phys. Rev. Lett. **83**, 3514 (1999).
[17] A. F. Isakovic, P. G. Evans, J. Kmetko, K. Cicak, Z. Cai, B. Lai, and R. E. Thorne, Phys. Rev. Lett. **96**, 046401 (2006).
[18] E. Pinsolle, N. Kirova, V. L. R. Jacques, A. A. Sinchenko, and D. LeBolloc'h, Phys. Rev. Lett. **109**, 256402 (2012).
[19] M. P. Maher, T. L. Adelman, J. McCarten, D. A. DiCarlo, and R. E. Thorne, Phys. Rev. B **43**, 9968 (1991).
[20] J. C. Gill, Solid State Commun. **39**, 1203 (1981).
[21] R. M. Fleming and L. F. Schneemeyer, Phys. Rev. B **33**, 2930 (1986).
[22] See Supplemental Material at http://link.aps.org/supplemental/10.1103/PhysRevLett.114.016404, which includes Refs. [23] and [24], for additional details on samples, measurement methods, and the origin of the asymmetry in the transient response.
[23] R. E. Thorne, Phys. Rev. B **45**, 5804 (1992).
[24] N. Beev and M. Kiviranta, Rev. Sci. Instrum. **83**, 066107 (2012).
[25] K. L. Ringland, A. C. Finnefrock, Y. Li, J. D. Brock, S. G. Lemay, and R. E. Thorne, Phys. Rev. Lett. **82**, 1923 (1999).
[26] H. Fukuyama and P. A. Lee, Phys. Rev. B **17**, 535 (1978); P. A. Lee and T. M. Rice, *ibid.* **19**, 3970 (1979).
[27] X.-D. Xiang and J. W. Brill, Phys. Rev. B **39**, 1290 (1989).